Meniscus-Mediated Organization of Colloidal Nanoparticles

Emmanuelle Pauliac-Vaujour and Philip Moriarty*

The School of Physics and Astronomy, The University of Nottingham, Nottingham NG7 2RD, U.K.

Received: May 29, 2007; In Final Form: August 20, 2007

We put forward a new strategy to elucidate and guide the processes underlying the organization of colloidal nanoparticles. The high wettability of toluene on a Teflon ring causes a nanoparticle solution on a silicon substrate to adopt a *meniscus*, rather than a droplet, shape. This simple ring configuration enables a systematic investigation of the interplay of contact-line dynamics and evaporation in pattern formation in nanoparticle assemblies.

I. Introduction

Far-from-equilibrium dynamics in colloidal nanoparticle solutions can, when appropriately controlled,[1,2] yield remarkably well-ordered close-packed lattices of particles. More generally, however, a plethora of nonequilibrium self-organized structures form,[3] including isolated droplets,[4−6] worm-like domains,[4,5,7] labyrinthine assemblies,[4,5,8] rings,[9−12] and cellular networks.[7,8,12−14] Although many of these experimentally observed structures can be reproduced within the elegant model developed by Rabani et al.[5] (with subsequent modifications by Yosef and Rabani[10] and Martin et al.[12,14]), there remain many important questions regarding the detailed dynamics of the nanoparticle−solvent system and, in particular, the roles of both evaporative and disjoining pressure-driven dewetting.

The deposition of nanoparticles onto a surface is usually carried out by evaporation of a drop of volatile solvent-based solution in open air or by spin-casting. In the general drop-deposition case, dewetting occurs and the solvent front retreats, leaving the particles adsorbed on the surface at the contact line (the "coffee-stain" effect).[15,16] In the case of spin-casting, the arrangement formed by the particles is usually uniform over most of the surface, but because of the rapid evaporation process, the system is trapped very far from equilibrium. For both drop-deposition and spin-casting, the deposited particles self-organize into a very broad variety of patterns originating from organization either at the solvent−substrate interface in the final stages of dewetting,[5] at the solvent−air interface,[2,17] or, as recently suggested by Yosef and Rabani[10] and Martin et al.,[12] due to a combination of evaporation at the solvent−substrate interface (driving the growth of nucleated holes in the solvent) *and* evaporation of the bulk solvent film.

Underlying the generation of such a broad range of nonequilibrium nanoparticle structures is the dynamic behavior of solvent dewetting and its coupling to the motion of the nanoparticles. Perhaps the most-striking examples to date of the exploitation of dewetting to control nanoparticle organization are the experiments of Xu et al.[18,19] and Huang et al.[20] In both cases, clever control of the motion of the dewetting front, that is, the solvent−substrate−air contact line, or, more succinctly, the triple line, was used to produce remarkably well-ordered pseudo-1D stripes of nanoparticles with widths and spacings on the order of micrometers (or, in the best cases, submicrometers). Xu et al.'s strategy involves the use of a sphere-on-flat arrangement to restrict the solvent to a particular confined geometry, promoting a highly regular pinning−depinning ("slip−stick") motion of the contact line. An interesting question, however, and one we address here, relates to the influence of the overall geometry of the solvent film and the associated contact line on the subsequent dewetting dynamics and pattern formation processes.

In this paper, we show that a deposition technique borrowed from previous work on latex spheres[21,22] (but, as we will describe below, involving substantially different physics) enables a systematic study of the role of evaporation time and contact-line dynamics on the organization of colloidal nanoparticles. A Teflon ring is used to impose a meniscus shape on the solvent−nanoparticle solution, a geometry that can be considered the "inverse" of that used in conventional drop-deposition (see Figure 1). We use tapping-mode atomic force microscopy (TM-AFM) to image the patterns formed at various distances from the center of this ring, enabling the effects of differences in evaporation time to be controllably studied on a *single* sample. A smooth and highly reproducible gradation from isolated droplets to close-packed and essentially void-free nanoparticle monolayers is observed as a function of radial distance. In addition, video microscopy provides key insight into the dynamics of the three-phase contact line as the solvent evaporates. The introduction of excess thiol ligands, a key ingredient in the production of highly ordered nanoparticle superlattices from drop deposits,[1,2] considerably enhances spatiotemporal instabilities in the motion of the contact line.

II. Experimental Details

We study solutions of 2-nm-diameter thiol-passivated gold nanoparticles suspended in toluene, synthesized according to the two-phase procedure developed by Brust et al.[23] in 1994. For reasons discussed below, in some cases excess thiol is added to a solution. The excess thiol is then chosen to match that used to passivate the particles (e.g., an excess of dodecanethiol will be added to a solution of dodecanethiol-passivated particles). The solution was deposited inside a PTFE (Teflon) ring onto a silicon oxide-terminated silicon substrate (see Figure 1) with the oxide either ∼2 nm thick (a native oxide) or a thermally grown ∼200-nm-thick film.[24,32] This technique exploits the

* Corresponding author. E-mail: philip.moriarty@nottingham.ac.uk. Tel.:+44 115 9515156. Fax:+44 115 9515180. www.nottingham.ac.uk/physics/research/nano.

10.1021/jp074152t CCC: $37.00
Published on Web 10/09/2007

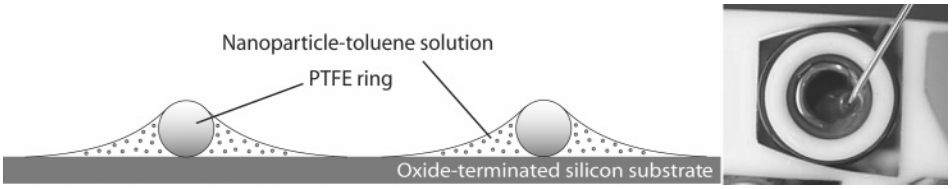

Figure 1. (left) Schematic of meniscus formation for nanoparticle solutions; (right) photograph of the nanoparticle solution being injected inside an 8-mm-inner-diameter PTFE ring lying on top of a silicon substrate.

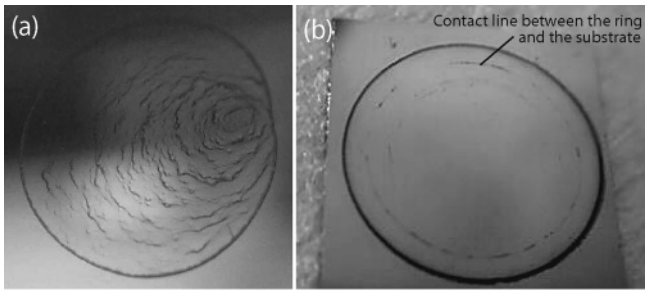

Figure 2. (a) Photograph of a 1×1 cm^2 silicon sample onto which a 10-μL drop of nanoparticle solution has been left to evaporate in open air. (b) Photograph of a 1.5×1.5 cm^2 silicon sample onto which solution has been deposited using an 8-mm (ID) Teflon ring, and left to dry in open air for 1 h, then placed under vacuum to make sure all of the remaining solvent has been removed.

preferential wetting of toluene on the Teflon ring (as compared to the underlying silicon oxide). A 30-μL drop of solution deposited within an 8-mm inner diameter (ID) Teflon ring that lies, unclamped, on top of the substrate forms a meniscus rather than a drop, as illustrated in Figure 1. A gradient is created in solvent thickness from the center to the edge of the ring. This enables a controlled study on a single sample of the effects of rapid versus slow solvent evaporation on gold nanoparticle self-organization. Although all visible solvent (i.e., that not located directly under the ring) usually disappears within 5−20 min, a small amount of solution can remain trapped for several hours under the Teflon. As a result, the samples are placed under vacuum for at least 12 h (following 1 h of drying in open air) to remove all residual solvent.[1]

An Asylum Research MFP-3D AFM system operating in intermittent contact mode with closed-loop control was used to image the resulting nanoparticle assemblies. Olympus AC240 silicon probes (spring constant, 2 Nm^{-1}; resonant frequency, 70 kHz) were used to acquire all data shown. A standard webcam with a frame rate of 10−15 frames per second (fps) (VGA) was used with the Virtual Dub software package to monitor the motion of the contact line during solvent dewetting.

III. Results and Discussion

It is first worth comparing the macroscopic morphology of nanoparticle films prepared using simple drop-deposition and the meniscus technique outlined in the previous sections. Figure 2 shows the dramatic differences observed in film homogeneity for the two techniques, with the "coffee-staining" effect resulting from drop-deposition clearly visible as the irregularly spaced rings in Figure 2a. In Figure 2b, which shows the sample morphology following evaporation of solvent within the ring geometry of Figure 1, macroscopic aggregates of particles form only near the region where the ring and the sample are in contact.

For a nanoparticle solution without an excess of thiol ligands, dewetting occurs in the center of the Teflon ring after ∼10−20 s (for a 15-μL drop of solution deposited within a 5-mm inner diameter (ID) Teflon ring). With the addition of an excess of dodecanethiol[1,2] (0.1% by volume), the initial dewetting time at the center of the ring increases to a few minutes. AFM images of the region at the center of the ring show that the relatively short time for evaporation (see Figure 4) leads to the type of small worm-like domains predicted by the Rabani et al.[5] model in the (spinodal) limit of homogeneous solvent evaporation. The liquid front then starts retreating slowly toward the edge of the ring, where the thicker solvent film leads to longer evaporation times. Videos of the motion of the dewetting front (i.e., the contact line) are included as Supporting Information (SI): video 1 (no excess thiol) and video 2 (with excess thiol). As discussed below, we also include a video of the motion of the contact line for a toluene−thiol solution containing no nanoparticles (SI video 3). Because of the contact-line dynamics associated with the presence of the nanoparticles (and, for video 2, excess thiol molecules) in the solvent, the progression of the front is rather erratic in space and time. For the case where free excess ligands are added to the solution, the dewetting front motion undergoes important and striking instabilities (SI video 2). First, the position of the contact line oscillates so that the progression of the front and the adsorption of the particles on the surface become very complex phenomena. Second, transverse fluctuations can sometimes develop and grow at the contact line, leading to the formation of a fingering instability at the macroscopic scale[11,18] (Figure 3).

An important question to address is whether the striking contact-line instabilities observed in SI video 2 are due to the combined effects of excess thiol and nanoparticles or whether excess thiol alone is sufficient to generate the oscillations we observe. In SI video 3, we show a video of the drying of a toluene−C_8 thiol (0.3% by volume) solution on native oxide-terminated Si(111). SI video 4 is a video of the drying of an equivalent volume of a pure toluene droplet for comparison. SI video 3 shows that the addition of thiol molecules, in the absence of nanoparticles, is sufficient to generate remarkably strong contact-line oscillations. We stress that the motion of the contact line in SI video 3 is not described adequately by the term slip−stick. It is clear in SI video 3 (particularly during the first 40 s or so of the video) that the motion of the contact line regularly *changes direction*. As pointed out by Qu, Suter, and Garoff,[24] a change in the direction of contact-line motion can only result from a modification of the Young's force at the contact line. The presence and, importantly, interactions of the surfactant molecules at (or close to) the contact line (i.e., the solid−liquid, liquid−vapor, and solid−vapor interfaces) drives a change in both the value and the temporal evolution of the Young's force. This effect differs from a pure slip−stick motion driven by nanoparticle/solute aggregation at the contact line, although in our case both slip−stick and oscillatory motion may occur during the dewetting process. To highlight the difference in contact-line dynamics for evaporating toluene−thiol and pure toluene drops, we have included as Supporting Information a plot of contact-line displacement versus time for each system.

The influence of surfactants on contact-line dynamics for spreading and evaporating liquid drops on solid (and liquid)

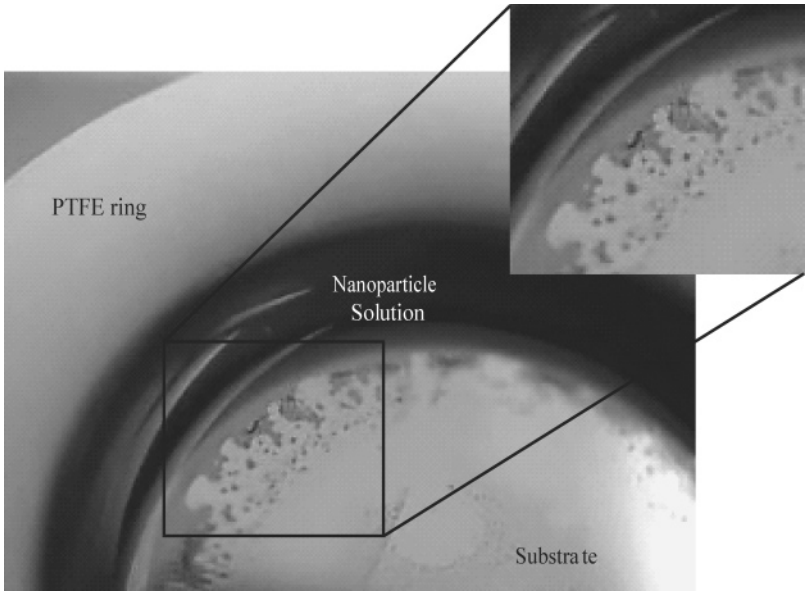

Figure 3. Photograph of a 1.5 × 1.5 cm^2 silicon sample onto which concentrated C_{12} nanoparticle solution, with an excess of 0.1% of thiol (in volume), has been deposited using an 8-mm (ID) Teflon ring. The picture is taken during the drying process, as the front retreats from the center of the ring toward its edge. The light regions in the image represent the bare silicon substrate, the gray regions comprise nanoparticles deposited from solution, and the black region is the retracting nanoparticle solution (identified in the figure). Fingering instabilities similar to those described by Maillard et al.[11] and Xu et al.[18] are visible.

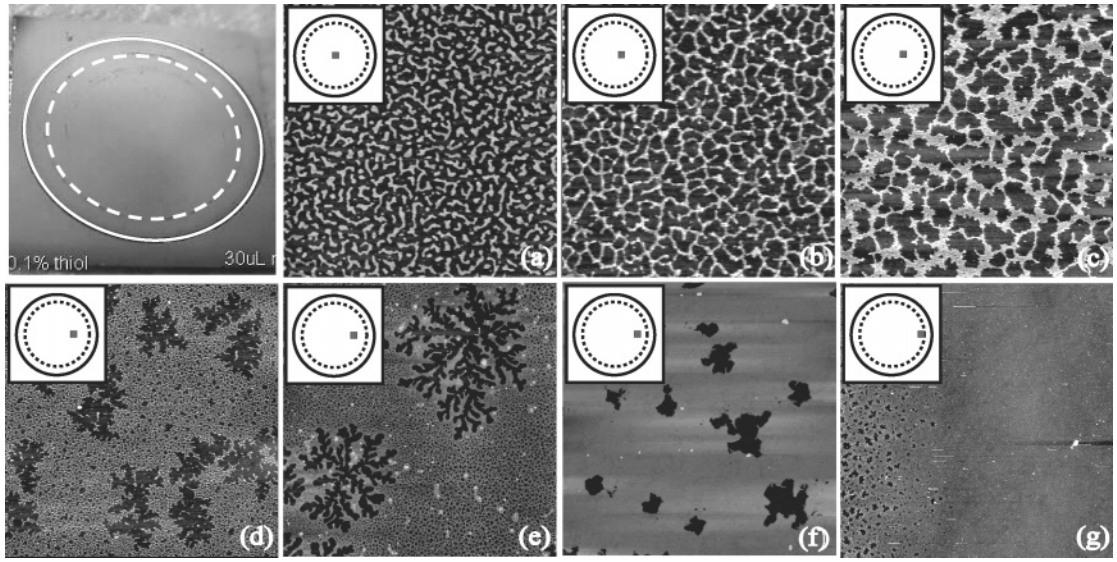

Figure 4. (a−f) Intermittent contact-mode AFM images of various dodecanethiol-passivated gold nanoparticle arrangements on a native oxide-terminated silicon sample prepared with the meniscus technique (top-left photograph). The solution used contained 0.1% excess dodecanethiol by volume. The insets indicate the (macroscopic) region on the sample where the scan is taken; the full circle represents the outer drying line, and the dashed line represents the contact line between the ring and sample. Scans a−c and f are 5 × 5 μm^2 in size; d, e, and g are 20 × 20 μm^2. Note that the thickness of the nanoparticle layer in each case is ∼3 nm, i.e., the approximate height expected for a single-particle-thick film. For images a and b, radially averaged Fourier transforms yielded mean feature separations of ∼250 and ∼200 nm, respectively.

substrates has been investigated in detail by a number of authors.[24−31] A variety of phenomena can couple to produce complex dynamics at the contact line and the associated precursor film. Truskett and Stebe[25] emphasize the importance of surfactant-mediated Marangoni−Bénard flow within the droplet. Others[24,26] have focused on the role of surfactant self-assembly. The closely related phenomena of *superspreading* and *autophobing* have also been studied in some depth,[24,27,31] although very many open questions remain. From the experiments described in this paper, addition of thiol to a toluene−nanoparticle solution very strongly affects the contact-line motion and thus the dynamics of nanoparticle assembly. Despite this, the *gradation* of nanoparticle patterns (from isolated droplets through to either complete or close-to-complete monolayers) remains broadly similar for thiol-free and excess thiol−nanoparticle solutions.

Although the front retreats relatively quickly at the beginning of the dewetting process, it very rapidly slows down while moving toward the edge of the ring. With no excess thiol, an 8-mm ID ring, and octanethiol-terminated 2-nm particles, although the *average* speed of the dewetting front is 5 μms^{-1}, the speed for the first minute of the dewetting process is 7.5 μms^{-1}, whereas for the final minute the dewetting front moves at ∼3.3 μms^{-1}. The corresponding values for the same solution with a 0.1% by volume addition of excess thiol are 5 μms^{-1}, 12.5 μms^{-1}, and 2.7 μms^{-1}. It is particularly interesting to note that past the initial dewetting stage the duration of solvent evaporation within the Teflon ring is not strongly affected by

the addition of excess thiol. Truskett and Stebe[25] have made a similar observation for an insoluble surfactant (pentadecanoic acid) on an aqueous droplet; the presence of the surfactant did not affect the mean evaporation rate of the droplet. Moreover, under our experimental conditions, we have thus far not succeeded in directly observing the formation of nanoparticle islands at the solvent−air interface (seeded by excess thiol) as described by Bigioni et al.[2] What is clear from the videos included as Supporting Information is that the addition of excess thiol plays a key role in the dynamics of dewetting in the final stages of drying. What is perhaps somewhat surprising is that the thiol-induced modification of the contact-line dynamics does not affect the overall gradation of nanoparticle patterns from the center, to the edge, of the ring. However, as described below, the presence of excess thiol certainly plays a role in determining the morphological characteristics of individual patterns.

Figure 4 shows the results obtained for dodecanethiol-passivated 2-nm Au nanoparticles deposited (from a solution with a 0.1% excess of dodecanethiol) onto a native-oxide terminated Si(111) substrate using the meniscus technique. A range of patterns, reminiscent of those seen on various samples prepared by spin-casting, are observed coexisting on a single sample. Because the evaporation time and the concentration of the solution vary across the substrate (due to the motion of the contact line), each "step" of the evaporation is associated with a given type of pattern. Thus, on a single sample one can observe patterns as varied as worm-like structures (toward the center, Figure 4a), cellular networks (sometimes on several different length scales) such as those shown in Figure 4b and c, branching structures that appear as one moves further out toward the edge of the ring (Figure 4d and e), up to the point, right at the edge of the ring, where monolayers with few or no holes at all finally form (Figure 4f and g). The images shown in Figure 4 have been obtained with a solution containing an excess of 0.1% of dodecanethiol in volume. Similar results can be obtained for a solution free of excess thiol, with the exception of the formation of large (tens of micrometers on a side) areas of close-packed monolayers (e.g., Figure 4g). Void-free monolayers have been observed only in the presence of excess ligands.[1] Following the discussions above, we tentatively postulate that it is the thiol-induced modification of the wettability of the solvent that plays the key role in reducing the void density. Recent simulations by both Yosef and Rabani[10] and our group,[12] based on the Rabani et al. Monte Carlo algorithm,[5,14] show that the inclusion of disjoining pressure-induced dewetting (in addition to evaporative dewetting) is key in order to reproduce a range of nanoparticle patterns formed in the late stages of drying. The local evaporation rate is of course dependent on solvent wettability. Thus, although the overall evaporation time is very similar for solutions that are free of thiol and those with an added excess of thiol, *local* wettability and evaporation rates may be strongly influenced by the addition of thiol.

Worm-like structures and cellular networks in gold nanoparticle assemblies have been studied extensively in the past.[3,6,7,11,13,14] A detailed study of the fingering structures (highly reminsicent of those observed for viscous fingering, crystallization from a melt, and diffusion-limited aggregation) seen in Figure 4d and e is outside the scope of this paper and will be the subject of a future publication.[34] We highlight, however, three key points related to the fingering patterns that are relevant to meniscus-driven nanoparticle organization: the isolated well-developed branching structures seen in Figure 4e have not been observed in spin-cast samples; (ii) fingered/branched structures form in a regime where there is an appreciable nanoparticle concentration and the time for solvent evaporation is relatively long; (iii) a key aspect of Rabani and Yosef's[10] model of finger formation in nanoparticle films relates to the effective competition between evaporation occurring at the edge of a hole nucleated at the substrate−liquid interface and evaporation of the bulk solvent film. An inspection of Figure 4e shows that the branched structures are surrounded by a void-ridden film very similar to the network structures formed at the solvent−substrate interface in the heterogeneous nucleation regime described by Rabani et al.[5,14] Moreover, the addition of excess thiol promotes the formation of more-developed branching patterns.

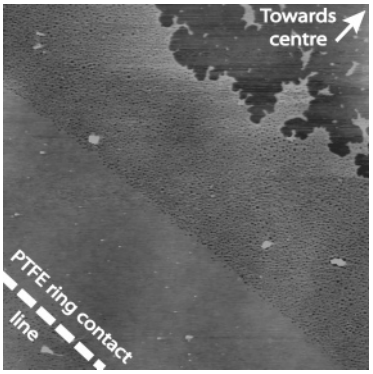

Figure 5. AFM image showing a clear transition between regions exhibiting different void concentrations: the boundary is very sharp and follows the shape of the Teflon ring. The approximate location of the contact point between the ring and the sample is represented by the thick dashed line. The size of the scan is $50 \times 50\ \mu m^2$.

Focusing now on the formation of close-packed monolayers, we highlight that these appear only at the edge of the Teflon ring, within a 5−25 μm wide area, along the circumference of the ring. We have found no clear dependence of the width of the circular monolayer on the amount of excess thiol added. However, in the ring configuration, monolayers will generally not form for volumes of excess thiol above a few 0.1%. The concentration of the solution also has to be adjusted in order to provide a sufficient coverage to lead to the formation of a close-packed monolayer. Increasing the concentration further will not increase the area of the close-packed layer. Instead, higher layers start to form and the excess solute (i.e., nanoparticles) aggregates mostly at the edge of the ring in the final stages of drying.

An intriguing phenomenon was observed at the boundary between regions exhibiting different types of patterns (especially close to the edge of the ring, where these regions are significantly thinner). These transitions are usually very abrupt, as illustrated in Figure 5. We believe that the clear boundary between a void-free and a void-ridden region in Figure 5 represents a slip−stick step undergone by the solvent front as it retreats toward the edge of the ring. At each step, the particles suspended in the part of the meniscus closest to the center of the sample, and where the thickness of liquid is close to that of a monolayer of particles, will be adsorbed abruptly on the surface over a circular area several tens of micrometers wide, as the front retreats by a similar distance. From one step to the next, the concentration of the solution becomes higher, leading to the formation of denser particle arrangements in the consecutive circular regions, following the correlations observed previously in spin-cast samples.[3,14] The clear line separating adjacent regions corresponds to a sudden motion of the contact line induced due to either a slip−stick motion or an excess thiol-mediated oscillation similar to that shown in SI video 3. The width of these steps reduces as the front approaches the ring,

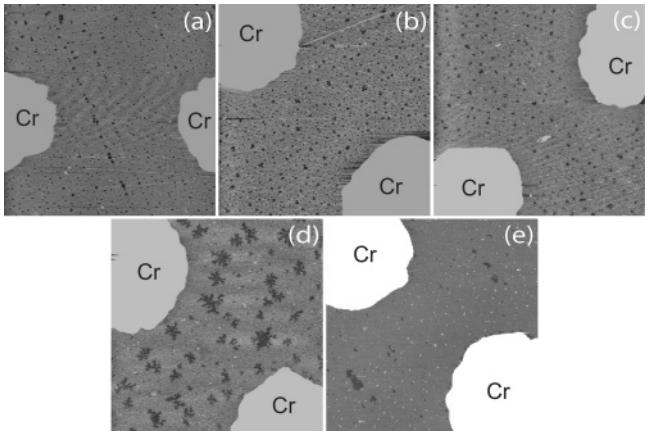

Figure 6. AFM scans showing dense nanoparticle arrangements between 20-nm-high Cr electrodes (indicated on each image). 15 μL of octanethiol-passivated nanoparticle solution with an excess of 0.1% octanethiol in volume were deposited using a 5.1-mm (ID) PTFE ring of thickness 1.6 mm on a 200-nm-thick thermally grown silicon oxide-terminated substrate. The images show successive nanoparticle arrangements obtained on a single sample as the distance of the contacts to the center of the sample is increased. The radial positions of the gaps between the electrodes from a to e are, respectively, 2.2, 2.3, 2.5, 2.7, and 3.0 mm. All scans are 20 $\times$ 20 μm^2.

as can be seen visually while monitoring the evaporation by video camera (see SI videos 2 and 3).

Finally, the ability to obtain a variety of different arrangements of gold nanoparticles on a single sample has significant potential with regard to elucidating the effects of network topology/morphology on electrical transport characteristics.[8] An important first step, however, is to determine the extent to which the presence of electrodes affects solvent dewetting dynamics within the Teflon ring. We deposited 10-μm-wide, 20-nm-high Cr electrodes onto a 200-nm-thick thermally grown silicon oxide (on a silicon substrate) via optical lithography. A total of eight pairs of electrodes were radially positioned and evenly spaced with regard to the center of the Teflon ring. Figure 6 shows examples of nanoparticle arrangements obtained between 10-μm-wide electrodes separated by a 10-μm gap for octanethiol-poassivated nanoparticle solutions (with an excess of 0.1% C_8 thiol). Figure 6e shows an example of a close-packed monolayer obtained when adding an excess of 0.1% of thiol in volume to a solution of octane−thiol passivated nanoparticles. In each case, it is clear that significant solvent dewetting does not occur close to the contacts: there are no denuded regions in the vicinity of the Cr electrodes.

IV. Conclusions

In summary, a meniscus geometry has been used to modify the dewetting dynamics of a solvent−nanoparticle solution from that associated with the conventional drop-deposition experimental geometry. The higher wettability of toluene on Teflon as compared to silicon oxide produces a solvent film that thins toward the center of a PTFE ring used to contain the solvent. Solvent dewetting initiates in the center of the ring. AFM images show that as the dewetting front moves toward the edge of the Teflon ring differences in local evaporation time and contact-line dynamics lead to a strong and systematic dependence of the type of nanoparticle assembly formed (e.g., droplets, networks, close-packed monolayers) on the radial distance from the center of the ring. Instabilities in the movement of the dewetting front (the triple line) are accentuated dramatically by the addition of excess thiol. The slip−stick and/or oscillatory motion of the contact line produces very sharp boundaries between different types of nanoparticle assemblies. When combined with radially arranged sets of electrode pairs, the meniscus/ring geometry enables a broad variety of nanoparticle patterns to be electrically contacted on a single sample.

Acknowledgment. We gratefully acknowledge funding from the European Union's Framework 6 Programme: Marie Curie Research Training Networks, contract MRTN-CT-2004-005728 (PATTERNS). We also thank the members of the PATTERNS network for helpful discussions regarding pattern formation in nanoparticle assemblies including, in particular, James Sharp (who originally brought ref 21 to our attention), Uwe Thiele, Ullrich Steiner, and Mathias Brust. In addition, E.P.-V. thanks Klara Elteto, from the James Franck Institute and Department of Physics (Chicago), for helpful discussion regarding the experimental details of the drop-deposition technique.

Supporting Information Available: Videos showing the motion of the contact line during solvent evaporation are available for download. Video 1 was taken for a solution of octanethiol-passivated 2-nm Au nanoparticles in toluene free of excess thiol, whereas video 2 shows the behavior of the same nanoparticle solution with a 0.3% by volume excess of octanethiol. Videos 3 and 4 show the motion of the contact line for a nanoparticle-free solution of thiol in toluene and for toluene alone, respectively. This material is available free of charge via the Internet at http://pubs.acs.org.

References and Notes

(1) Lin, X. M.; Jaeger, H. M.; Sorensen, C. M.; Klabunde, K. J. *J. Phys. Chem. B* **2001**, *105*, 3353−3357.

(2) Bigioni, T. P.; Lin, X. M.; Nguyen, T. T.; Corwin, E. I.; Witten, T. A.; Jaeger, H. M. *Nat. Mater.* **2006**, *5*, 265−270.

(3) Martin, C. P.; Blunt, M. O.; Vaujour, E.; Fahmi, A.; D'Aleo, A.; De Cola, L.; Vögtle, F.; Moriarty, P. Self-Organised Nanoparticle Assemblies; A Panoply of Patterns. In *Systems Self-Assembly: Interdisciplinary Snapshots*; Krasnogor, N., Gustafson, S., Pelta, D., Verdegay, J. L., Eds.; Elsevier, in press, 2007.

(4) Ge, G.; Brus, L. *J. Phys. Chem. B* **2000**, *104*, 9573−9575.

(5) Rabani, E.; Reichman, D. R.; Geissier, P. L.; Brus, L. E. *Nature* **2003**, *426*, 271−274.

(6) Blunt, M. O.; Martin, C. P.; Ahola-Tuomi, M.; Pauliac-Vaujour, E.; Sharp, P.; Nativo, P.; Brust, M.; Moriarty, P. *Nat. Nanotechnol.* **2007**, *2*, 167−170.

(7) Moriarty, P.; Taylor, M. D. R.; Brust, M. *Phys. Rev. Lett.* **2002**, *89*, 248303.

(8) Blunt, M. O.; Suvakov, M.; Pulizzi, F.; Martin, C. P.; Pauliac-Vaujour, E.; Stannard, A.; Rushforth, A.; Tadic, B.; Moriarty, P. *Nano Lett.* **2007**, *7*, 855−860.

(9) Ohara, P. C.; Gelbart, W. M. *Langmuir* **1998**, *14*, 3418−3424.

(10) Yosef, G.; Rabani, E. *J. Phys. Chem. B* **2006**, *110*, 20965−20972.

(11) Maillard, M.; Motte, L.; Pileni, M. P. *Adv. Mater.* **2001**, *13*, 200−204.

(12) Martin, C. P.; Blunt, M. O.; Pauliac-Vaujour, E.; Stannard, A.; Moriarty, P.; Vancea, I.; Thiele, U. *Phys. Rev. Lett.* **2007**, *99*, 116103.

(13) Maillard, M.; Motte, L.; Ngo, A. T.; Pileni, M. P. *J. Phys. Chem. B* **2000**, *104*, 11871−11877.

(14) Martin, C. P.; Blunt, M. O.; Moriarty, P. *Nano Lett.* **2004**, *4*, 2389.

(15) Deegan, R. D.; Bakajin, O.; Dupont, T. F.; Huber, G.; Nagel, S. R.; Witten, T. A. *Nature* **1997**, *389*, 827−829.

(16) Deegan, R. D. *Phys. Rev. E* **2000**, *61*, 475−485.

(17) Narayanan, S.; Wang, J.; Lin, X.-M. *Phys. Rev. Lett.* **2004**, 2004, *93*, 135503.

(18) Xu, Jun; Xia, Jianfeng; Lin, Zhiqun *Angew. Chem., Int. Ed.* **2007**, *46*, 1860−1863

(19) Xu, J.; Xia, J.; Hong, S. W.; Lin, Z. Q.; Qiu, F.; Yang, Y. L. *Phys. Rev. Lett.* **2006**, *96*, 066104.

(20) Huang, J.; Kim, F.; Tao, A. R.; Connor, S.; Yang, P. *Nat. Mater.* **2005**, *4*, 896−900.

(21) Gigault, C.; Dalnoki-Veress, K.; Dutcher, J. R. *J. Colloid Interface Sci.* **2001**, *243*, 143−155.

(22) Denkov, N. D.; Velev, O. D.; Kralchevsky, P. A.; Ivanov, I. B.; Yoshimura, H.; Nagayama, K. *Langmuir* **1992**, *8*, 3183−3190.

(23) Brust, M.; Walker, M.; Bethell, D.; Schiffrin, D. J.; Whyman, R. *J. Chem. Soc. Chem. Commun.* **1994**, 426.
(24) Qu, D.; Suter, R.; Garoff, S. *Langmuir* **2002**, *18*, 1649−1654.
(25) Truskett, V. N.; Stebe, K. J. *Langmuir* **2003**, *19*, 8271−8279.
(26) Varanasi, K. S.; Garoff, S. *Langmuir* **2005**, *21*, 9932−9937.
(27) Craster, R. V.; Matar, O. K. *Langmuir* **2007**, *23*, 2588−2601.
(28) Gokhale, S. J.; Plawsky, J. L.; Wayner, P. C. *Langmuir* **2005**, *21*, 8188−8197.
(29) Chan, K. Y.; Borhan, A. *J. Colloid Interface Sci.* **2005**, *287*, 233−248.
(30) Jensen, O. E.; Naire, S. *J. Fluid Mech.* **2006**, *554*, 5−24.
(31) Afsar-Siddiqui, A. B.; Luckham, P. F.; Matar, O. K. *Langmuir* **2004**, *20*, 7575−7582.
(32) We note that the silicon oxide thickness directly affects the relevant Hamaker constant (see Seemann, R.; Herminghaus, S.; Jacobs, K. *Phys. Rev. Lett.* **2001**, *86*, 5534) and, thus, the dewetting patterns.[33] However, the general trend of the patterns formed within the Teflon ring remains the same: isolated droplets/worm-like domains at the center, through to close-packed layers at the edge of the ring.
(33) Pauliac-Vaujour, E.; Stannard, A.; Martin, C. P.; Blunt, M. O.; Moriarty, P. To be submitted for publication, 2007.
(34) Pauliac-Vaujour, E.; Stannard, A.; Martin, C. P.; Vancea, I.; Thiele, U.; Moriarty, P. To be submitted for publication.